Analysis of two parameter identification methods for original and modified Johnson-Cook fracture strains, including numerical comparison and validation of a new blue-brittle dependent fracture model for free-cutting Steel 50SiB8

Author(s):
Gerstgrasser, Marcel; Smolenicki, Darko; Akbari, Mansur; Klippel, Hagen; Roelofs, Hans; Cadoni, Ezio; Wegener, Konrad

Publication date:
2021-04

Permanent link:
https://doi.org/https://doi.org/10.3929/ethz-b-000461714

Theoretical and Applied Fracture Mechanics 112 (2021) 102905

Contents lists available at ScienceDirect

Theoretical and Applied Fracture Mechanics

journal homepage: www.elsevier.com/locate/tafmec

Analysis of two parameter identification methods for original and modified Johnson-Cook fracture strains, including numerical comparison and validation of a new blue-brittle dependent fracture model for free-cutting steel 50SiB8

Marcel Gerstgrasser [a,*,1], Darko Smolenicki [a,1], Mansur Akbari [b,*,1], Hagen Klippel [a,*,1], Hans Roelofs [c], Ezio Cadoni [d], Konrad Wegener [a,b]

[a] Institute of Machine Tools and Manufacturing, ETH Zurich, Leonhardstrasse 21, 8092 Zurich, Switzerland
[b] inspire AG, Technoparkstrasse 1, 8005 Zurich, Switzerland
[c] R&D, Swiss Steel AG, Emmenweidstr. 90, 6020 Emmenbrücke, Switzerland
[d] DynaMat Lab, University of Applied Sciences of Southern Switzerland, 6952 Canobbio, Switzerland

ARTICLE INFO

Keywords:
Forward and backward parameter identification methods
Constitutive behaviour
Rate-dependent material
Kolsky bar
Blue-brittleness fracture model
FE simulations

ABSTRACT

A non-linear relation between fracture strain and temperature is observed in Split Hopkinson Tension Bar (SHTB) tests for free-cutting steel 50SiB8 at high strains and high temperatures, due to blue-brittleness. A fourth-degree polynomial function for the thermal parts of the original and modified Johnson-Cook (JC) fracture strain constitutive equation is suggested and the corresponding parameters are identified. Fracture modelling of 50SiB8 is not reported in literature. 50SiB8 is characterized under quasi-static, isothermal, high temperature and high strain rate conditions using smooth and notched tension specimens. For the calculation of the original and modified JC fracture parameters, two different parameter identification procedures, so-called forward and backward parameter identification methods are performed, compared with each other and explained in detail. For the stress triaxiality factor of the original and modified JC fracture model, the forward parameter identification method is suggested for the original JC fracture model, while backward parameter identification method is proposed for the modified JC fracture model. The effect of blue-brittleness in the temperature factor and the corresponding parameters are presented. Furthermore, FEM simulations of the original and the blue-brittleness based JC fracture model are compared with experiments. In the blue-brittle temperature range, the new adjusted JC model shows more accurate results, regarding fracture diameter and strain. Additionally, this work introduces a fracture model combining the Bai-Wierzbicki stress triaxiality dependent model, JC fracture models and the nonlinear temperature factor with blue-brittleness effect, while further experiments are required in order to determine its parameters.

1. Introduction

There are several parameters that influence the fracture behaviour of materials. Hydrostatic stress and the associated stress triaxiality have strong influence on the fracture strain [1–4]. The void growth models and their recent enlargement have become the fundamentals of modern ductile fracture mechanics [5]. Based on the analysis of large growth and coalescence of microscopic voids under the superposition of hydrostatic stresses, the exponential expression for the corresponding equivalent fracture strain of the Rice and Tracey fracture model [2] is written as:

$$\varepsilon_f = D_{RT1} e^{D_{RT2}\eta} \tag{1}$$

where D_{RT1} and $D_{RT2}$are the material parameters and η is defined as stress triaxiality, which is represented by the ratio of negative hydrostatic pressure p to von Mises equivalent stress $\bar{\sigma}$, as shown in the following equations:

$$\eta = \frac{-p}{\bar{\sigma}} = \frac{\sigma_m}{\bar{\sigma}} \tag{2}$$

* Corresponding authors.
E-mail addresses: gerstgrasser@iwf.mavt.ethz.ch (M. Gerstgrasser), akbari@alumni.ethz.ch (M. Akbari), klippel@iwf.mavt.ethz.ch (H. Klippel).
[1] These authors contributed equally and share the first authorship.

https://doi.org/10.1016/j.tafmec.2021.102905
Received 11 August 2020; Received in revised form 10 December 2020; Accepted 5 January 2021
Available online 8 January 2021

Nomenclature

a	radius of the necking cross-section
A_0	initial cross-section area
A_f	cross-area after testing
c	coefficient
D_i, D_k	material parameter
Δ_k	trust-region radius
ε_f	equivalent strain at failure
$\dot{\varepsilon}_0$	reference strain rate
$\dot{\varepsilon}$	strain rate
ε_{f_0}	fracture strain at room temperature and quasi-static conditions for the smooth specimen
$\dot{\varepsilon}^*$	dimensionless strain-rate ratio
η	stress triaxiality
$f(x)$	smooth objective function
J_1, J_2,J_3	first, second and third deviatoric stress invariant
$J(x_k)$	Jacobian matrix
p	hydrostatic pressure
R	local radius of a neck in the round bar specimen
$r_i(x)$	residual function
RSS	residual sum of squares
σ_i	principal stresses
$\overline{\sigma}$	von Mises equivalent stress
σ_m	mean stress
T	temperature
T_0	room temperature
θ	Lode angle parameter
$\overline{\theta}$	normalized Lode angle parameter
T^*	homologous temperature
x_{data}	given input data
y_{data}	observed output data
$x(t)$	path, which proceeds to a local minimum to obtain the values of the material parameters

with

$$p = -\sigma_m = -\frac{1}{3}(\sigma_1 + \sigma_2 + \sigma_3) \tag{3}$$

$$\overline{\sigma} = \sqrt{\frac{1}{2}\left[(\sigma_1 - \sigma_2)^2 + (\sigma_2 - \sigma_3)^2 + (\sigma_3 - \sigma_1)^2\right]} = \sqrt{3J_2} \tag{4}$$

where σ_i for $i = 1, 2$ and 3 are the principal stresses and J_2 is defined as the second deviatoric stress invariant. In addition to the stress triaxiality influence, Bai and Wierzbicki [6] postulated a new asymmetric fracture locus, considering Lode angle dependence:

$$\varepsilon_f = \left[\frac{1}{2}\left(D_{BW1}\, e^{-D_{BW2}\,\eta} + D_{BW5}\, e^{-D_{BW6}\,\eta}\right) - D_{BW3}\, e^{-D_{BW4}\,\eta}\right]\overline{\theta}^2 + \frac{1}{2}\left(D_{BW1}\, e^{-D_{BW2}\,\eta} - D_{BW5}\, e^{-D_{BW6}\,\eta}\right)\overline{\theta} + D_{BW3}\, e^{-D_{BW4}\,\eta} \tag{5}$$

$$\overline{\theta} = 1 - \frac{6\theta}{\pi} \tag{6}$$

$$\theta = \frac{1}{3}arccos\left(\frac{3\sqrt{3}\,J_3}{2J_2^{3/2}}\right) \tag{7}$$

where the six material parameters D_{BW1} to D_{BW6} need to be identified, $\overline{\theta}$ and θ are the normalized and actual Lode angle [7], respectively and J_3 is defined as the third deviatoric stress invariant. Several researchers have investigated and included the behavior of stress triaxiality in conjunction with the Lode angle parameter to describe fracture more accurately [8–13]. A comprehensive derivation for equation (7) is demonstrated in [14]. According to Buchkremer and Schoop [15], the Lode parameter characterizes the loading direction, expressly tension, compression and shear. Bai et al. [5] indicated that the stress state at a point in an isotropic material can also be defined by a spherical coordinate system based on fracture strain ε_f, the stress triaxiality related coordinate and Lode angle θ.

The normalized Lode angle itself is in a range of $-1 \leqslant \overline{\theta} \leqslant 1$. For smooth and notched tensile axisymmetric bars, as used in this paper, the parameter $\overline{\theta}$ gets equal 1 with reference to Bai and Wierzbicki [6] and equation converts into

$$\varepsilon_f = D_{BW1}\, e^{-D_{BW2}\,\eta} \tag{8}$$

which is the same as the fracture model of Rice and Tracey [2] and the reduced first factor of the fracture strain constitutive equation from Johnson and Cook [4] (JC). According to Khan and Liu [16], who have also proposed a strain and temperature dependent fracture criterion for isotropic and anisotropic metals, the strain rate and temperature effects are not considered in [1,2,3,6,8,9,10,12,13]. The strain rate and temperature dependency is taken into account in the research of Johnson and Cook [4], the slightly modified version of the Johnson and Cook fracture strain equation, proposed by Børvik et al. [17], and in recent studies from Roth and Mohr [11], which have included only the strain rate in a loose analogy with the Johnson and Cook model through a coefficient in the Hosford-Coulomb model. The entire strain at fracture formula of the original and modified Johnson-Cook fracture model incorporates not only stress triaxiality, but also strain-rate and temperature factors. Bai and Wierzbicki [18] depicted that the JC fracture locus captures the effect of stress triaxiality on fracture strains well, but, due to change of the Lode angle parameter, the model does not include the loss of ductility. To resolve this problem, Buchkremer et al. [19] adjusted the first factor of the Johnson-Cook model to the symmetric Lode angle dependent Bai-Wierzbicki model in Eq. (5). Furthermore, for the case of final ductile fracture, the strain rate dependent second factor of the Johnson-Cook model is omitted in:

$$\varepsilon_f = \left[\left(D_{1BKV}e^{-D_{2BKV}\,\eta} - D_{3BKV}e^{-D_{4BKV}\,\eta}\right)\overline{\theta}^2 + D_3 e^{-D_{4BKV}\,\eta}\right]\left[1 + D_{5BKV}T^*\right] \tag{9}$$

$$T^* = \frac{T - T_0}{T_m - T_0} \tag{10}$$

where $D_{i\,BKV}$ for $i = 1, 2, 3, 4$ and 5 are the material parameters and $\overline{\theta}$ gets equal to 1 again for smooth and notched tensile round bars, which converts the first factor of Eq. (9) into the right hand side of Eq. (8). Compared to the first factor of the fracture strain constitutive equation from Johnson and Cook [4], the offset parameter is still missing. T^*, T_0 and T_m are the homologous, room and melting temperature, respectively.

Childs [20] has also analysed a Johnson-Cook type of pressure, strain rate and temperature dependent failure law in combination with blue-brittle behaviour. The temperature models are based on an insufficient temperature range from 20 to 500 °C, predicting a blue-brittle reduction of failure strain as temperature reaches 600 °C. Above 650 °C, the failure strain even becomes infinite, which clearly demonstrates an unrealistic and unnatural material behaviour. As Childs [20] has highlighted, more temperature tests in the high strain rate fields are needed. Therefore, a temperature range from 20 to 800 °C and a strain rate range from around 500 to 900 s^{-1} in the high temperature fields has been included for the Split Hopkinson Tension bar test in this study, to analyse and provide a more accurate fracture model taking the blue-brittleness effect into

account.

Including all five JC material parameters, the well-known standard material parameter identification procedure, which is called "forward parameter identification method" in this research, is performed by many researchers [4,21,17,22,23,24]. However, just a few researchers explicated the so-called "backward parameter identification method" only for the slightly modified Johnson and Cook fracture strain equation [25]. In the present research, in addition to the strain rate dependency and offset parameter, two different backward and forward parameter identification methods for the original and the modified fracture strain constitutive equation of Johnson and Cook [4] are analysed and compared, using a new type of graphitized free-cutting steel 50SiB8 provided by Swiss Steel AG. The material parameters of all variations are explicitly illustrated for 50SiB8 in this research. Nonlinear thermal behaviour for the free-cutting steel 50SiB8 with blue-brittleness effect is also investigated and the parameters of the fourth-degree polynomial function are obtained, considering the most convenient parameter identification method for each Johnson-Cook fracture strain constitutive equation, based on RSS-values. The original and blue-brittleness containing Johnson-Cook model are validated with FEM simulations, performed in Abaqus 6.14–1 with explicit solver, and compared with experiments. The blue-brittleness containing model provides better results in the above mentioned 600 °C temperature range. Additionally, a new fracture model is proposed, including the nonlinear temperature factor with blue-brittleness and the Lode angle dependent Bai-Wierzbicki model.

2. Original and modified fracture strain constitutive equation

Strain at fracture according to Johnson and Cook [4] can be expressed as:

$$\varepsilon_f = \left[D_1 + D_2\, e^{D_3\,\eta}\right]\left[1 + \ D_4\, ln\left(\frac{\dot{\varepsilon}}{\dot{\varepsilon}_0}\right)\right][1 + D_5\, T^*] \tag{11}$$

where ε_f is the equivalent strain at failure and D_1 to D_5 are material parameters. The first factor of the equation depends on the stress-triaxiality η, whereas the second and third factors depend on strain rate $\dot{\varepsilon}$ and temperature T, respectively. $\dot{\varepsilon}_0$ is defined as reference strain rate. The equivalent strain at failure in Eq. (11) is also commonly used in simulation of machining processes, such as in [26].

To avoid unwanted effects of the dimensionless strain-rate ratio $\dot{\varepsilon}^* = \dot{\varepsilon}/\dot{\varepsilon}_0 \ < 1$ in Eq. (11), Børvik et al. [17] have modified the strain rate sensitivity factor of the original Johnson and Cook fracture strain equation. The slightly modified JC fracture strain model is written as

$$\varepsilon_f = \left[D_1 + D_2\, e^{D_3\,\eta}\right][1 + \ \dot{\varepsilon}^*]^{D_4}[1 + D_5 T^*] \tag{12}$$

The reference strain rates $\dot{\varepsilon}_0$ for the original and modified JC fracture strain equation are set to 0.001 s^{-1} and 1 s^{-1}, respectively. The equivalent fracture strain at failure ε_f in the necking cross-section (axisymmetric bar) can be approximately computed by

$$\varepsilon_f = ln\left(\frac{A_0}{A_f}\right) \tag{13}$$

where A_0 and A_f are the cross-section areas of the specimens before and after the tensile test, respectively. The parameter of ε_f has to be calculated for all fractured specimens using different conditions to identify the material parameters D_i in equation (11) and (12), as explained in Sections 2.1 and 2.2. As well explained by Bai et al. [5], Bao [27] has revisited the analytical formula of Bridgman [28] using finite element simulation and proposed a corrected equation with a coefficient $\sqrt{2}$, to compute the stress triaxiality η for different notched specimens, as an improved and acceptable approximation:

$$\eta = \frac{1}{3} + \ \sqrt{2}\ ln\left(1 + \frac{a}{2R}\right) \tag{14}$$

where the local radius of a notch in the round bar specimen is R and the radius of the necking cross-section is a . In this research, the stress triaxiality calculations are based on the revised formula as shown in Eq. (14). The range of the stress state parameters in smooth or notched round bar specimen for tensile tests is $\eta \geqslant 1/3$, as reported in [5,27].

2.1. Forward parameter identification method

The flowchart of the forward parameter identification method for the original and modified JC fracture model are summarised in Fig. 1. To identify the material parameters D_1, D_2 and D_3 in the first factor of the original and modified JC fracture strain equation, quasi-static and isothermal tension tests are performed using different notched specimens. Under quasi-static and isothermal conditions, the fracture strain formula, in Eqs. (11) and (12), converts into

$$\varepsilon_f(\eta) = \left[D_1 + D_2\, e^{D_3\,\eta}\right] \tag{15}$$

where the natural logarithm of the strain rate ratio $ln\left(\dot{\varepsilon}/\dot{\varepsilon}_0\right)$ in the original JC fracture formula, the ratio $\dot{\varepsilon}/\dot{\varepsilon}_0$ in the modified equation approximately and the homologous Temperature T^* get equal to zero. The fracture strain with the corresponding Eq. (13) and the stress triaxiality, as shown in Eq. (14), are used for each test, to compute the three parameters with curve fitting.

The parameter D_4 is determined by performing high strain rate tension tests on smooth specimens at different strain rates and ambient temperature. Therefore in this case, Eq. (14) converts into η_{smooth} equal to the value of $1/3$ for $R \doteq \infty$ and Eq. (15) changes into a constant for the second factor of the fracture strain equation. The strain rate dependent fracture strain function for the original JC is written as:

$$\varepsilon_f(\dot{\varepsilon}) = \varepsilon_f(\eta_{smooth})\left[1 + \ D_4\, ln\left(\frac{\dot{\varepsilon}}{\dot{\varepsilon}_0}\right)\right] \tag{16}$$

and for the modified equation:

$$\varepsilon_f(\dot{\varepsilon}) = \varepsilon_f(\eta_{smooth})\left[1 + \ \frac{\dot{\varepsilon}}{\dot{\varepsilon}_0}\right]^{D_4} \tag{17}$$

where the homologous Temperature T^* is still zero and the fracture strain $\varepsilon_f(\dot{\varepsilon})$ with the corresponding strain rate is used to identify the parameter D_4 with curve fitting.

Using a similar procedure, the material parameter D_5 is calculated from different temperature tests with smooth tensile specimens at specific strain rates, which is more accurate than testing under quasi-static conditions. The temperature dependent fracture strain equation for the original and modified JC is expressed as:

$$\varepsilon_f(T) = \varepsilon_f(\eta_{smooth})\,\varepsilon_f(\dot{\varepsilon})\,[1 + D_5\, T^*] \tag{18}$$

where $\varepsilon_f(\dot{\varepsilon})$ includes the strain rates for each temperature test. The temperature dependent fracture strain $\varepsilon_f(T)$ and the corresponding temperature T are used for the identification of D_5.

2.2. Backward parameter identification method

The backward parameter identification method for the original and modified JC fracture model is summarised in Fig. 2. Børvik et al. [25] describes a possible backward parameter identification for the material parameters of the slightly modified Johnson-Cook model, starting with the parameter D_4. In this paper, the methodology is also adapted to the original JC fracture strain constitutive equation. Starting with the identification of the strain rate dependent parameter D_4 under isothermal conditions, the mathematical expression for the original JC

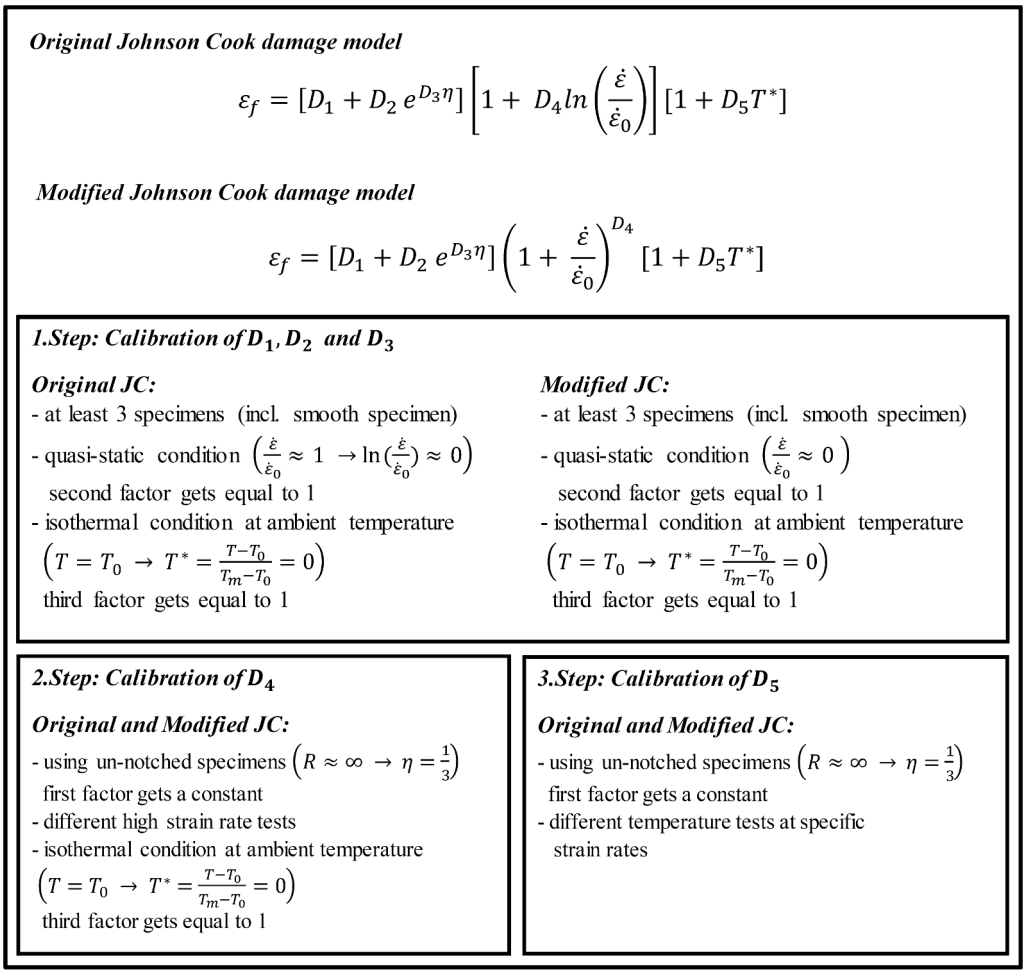

Fig. 1. Forward parameter identification of the original and modified JC fracture strain equation.

fracture strain function is written as:

$$\varepsilon_f(\dot{\varepsilon}) = \varepsilon_{f_0}\left(1 + D_4 ln\left(\frac{\dot{\varepsilon}}{\dot{\varepsilon}_0}\right)\right) \tag{19}$$

and for the modified equation:

$$\varepsilon_f(\dot{\varepsilon}) = \varepsilon_{f_0}\left(1 + \frac{\dot{\varepsilon}}{\dot{\varepsilon}_0}\right)^{D_4} \tag{20}$$

where ε_{f_0} is regarded as the fracture strain at room temperature and quasi-static conditions for the smooth specimen [25]. The homologous Temperature T^* is equal to zero and the fracture strain $\varepsilon_f(\dot{\varepsilon})$ with the corresponding strain rate is used to identify the fracture strain ε_{f_0} and parameter D_4.

The temperature parameter D_5 of the slightly modified model is identified by considering the actual strain rate in each temperature test [25]. The mathematical expression for the original JC equation is:

$$\varepsilon_f(\dot{\varepsilon}) = \varepsilon_{f_0}\left(1 + D_4 ln\left(\frac{\dot{\varepsilon}}{\dot{\varepsilon}_0}\right)\right)(1 + D_5\, T^*) \tag{21}$$

and for the modified JC strain rate dependent fracture strain function:

$$\varepsilon_f(\dot{\varepsilon}) = \varepsilon_{f_0}\left(1 + \frac{\dot{\varepsilon}}{\dot{\varepsilon}_0}\right)^{D_4}(1 + D_5\, T^*) \tag{22}$$

where the temperature dependent fracture strain $\varepsilon_f(T)$ is plotted against the temperature T for each strain rate to obtain D_5. Finally, the parameters from the first factor, which describes the influence of the triaxiality on the fracture strain, are determined by testing pre-notched specimens. The equation for the original JC stress triaxiality dependent fracture strain function, which also includes the quasi-static strain rate under isothermal conditions, is expressed as

$$\varepsilon_f(\eta) = \left[D_1 + D_2\, e^{D_3\,\eta}\right]\left[1 + D_4 ln\left(\frac{\dot{\varepsilon}}{\dot{\varepsilon}_0}\right)\right] \tag{23}$$

and for the modified JC

$$\varepsilon_f(\eta) = \left[D_1 + D_2\, e^{D_3\,\eta}\right]\left(1 + \frac{\dot{\varepsilon}}{\dot{\varepsilon}_0}\right)^{D_4} \tag{24}$$

where $ln\left(\dot{\varepsilon}/\dot{\varepsilon}_0\right)$ gets equal zero and the ratio $\dot{\varepsilon}/\dot{\varepsilon}_0$ gets approximately null, which convert Eqs. (23) and (24) into Eq. (15) again. Ultimately, the three stress triaxiality dependent material parameters D_1, $D_2$and D_3 are identified using curve fitting.

3. Material and experiments

As already mentioned in chapter 2, the following types of tensile tests are needed for the parameter identification of the original and modified JC fracture strain constitutive equation: quasi-static smooth as well as

Original Johnson Cook damage model

$$\varepsilon_f = [D_1 + D_2\, e^{D_3\eta}]\left[1 + D_4 ln\left(\frac{\dot{\varepsilon}}{\dot{\varepsilon}_0}\right)\right][1 + D_5 T^*]$$

Modified Johnson Cook damage model

$$\varepsilon_f = [D_1 + D_2\, e^{D_3\eta}]\left(1 + \frac{\dot{\varepsilon}}{\dot{\varepsilon}_0}\right)^{D_4}[1 + D_5 T^*]$$

1.Step: Calibration of D_4

Original JC:

- Using equation $\varepsilon_f(\dot{\varepsilon}) = \varepsilon_{f_0}\left[1 + D_4 ln\left(\frac{\dot{\varepsilon}}{\dot{\varepsilon}_0}\right)\right]$ entire first factor gets a parameter ε_{f_0}
- different high strain rate tests
- isothermal condition at ambient temperature $\left(T = T_0 \rightarrow T^* = \frac{T-T_0}{T_m-T_0} = 0\right)$ third factor gets equal to 1

Modified JC:

- Using equation $\varepsilon_f(\dot{\varepsilon}) = \varepsilon_{f_0}\left(1 + \frac{\dot{\varepsilon}}{\dot{\varepsilon}_0}\right)^{D_4}$ entire first factor gets a parameter ε_{f_0}
- different high strain rate tests
- isothermal condition at ambient temperature $\left(T = T_0 \rightarrow T^* = \frac{T-T_0}{T_m-T_0} = 0\right)$ third factor gets equal to 1

2.Step: Calibration of D_5

Original JC:

- Using equation $\varepsilon_f(T) = \varepsilon_{f_0}\left[1 + D_4 ln\left(\frac{\dot{\varepsilon}}{\dot{\varepsilon}_0}\right)\right][1 + D_5 T^*]$ with identified parameters ε_{f_0} and D_4
- different temperature tests at specific strain rates

Modified JC:

- Using equation $\varepsilon_f(T) = \varepsilon_{f_0}\left(1 + \frac{\dot{\varepsilon}}{\dot{\varepsilon}_0}\right)^{D_4}[1 + D_5 T^*]$ with identified parameters ε_{f_0} and D_4
- different temperature tests at specific strain rates

3.Step: Calibration of D_1, D_2 and D_3

Original JC:

- Using obtained parameter ε_{f_0} as a curve-point
- testing different pre-notched specimens under quasi-static conditions $\left(\frac{\dot{\varepsilon}}{\dot{\varepsilon}_0} \approx 1 \rightarrow \ln(\frac{\dot{\varepsilon}}{\dot{\varepsilon}_0}) \approx 0\right)$ second factor gets equal to 1
- isothermal condition at ambient temperature $\left(T = T_0 \rightarrow T^* = \frac{T-T_0}{T_m-T_0} = 0\right)$ third factor gets equal to 1

Modified JC:

- Using obtained parameter ε_{f_0} as a curve-point
- testing different pre-notched specimens under quasi-static conditions $\left(\frac{\dot{\varepsilon}}{\dot{\varepsilon}_0} \approx 0\right)$ second factor gets equal to 1
- isothermal condition at ambient temperature $\left(T = T_0 \rightarrow T^* = \frac{T-T_0}{T_m-T_0} = 0\right)$ third factor gets equal to 1

Fig. 2. Backward parameter identification of the original and modified JC fracture strain equation.

notched specimen tests at ambient temperature, in addition to SHTB tests at different strain rates and temperatures.

3.1. Material

Free-cutting steels with graphite inclusions, such as 50SiB8, are claimed to perform excellent in machining processes [29]. The graphite acts as a solid lubricant, creates small chips and is an environmentally friendly alternative to widely used sulphur. 50SiB8 has been produced at Swiss Steel AG, starting with the melting process in an electric arc furnace, followed by continuously casting. In a continuous furnace at Deutsche Edelstahlwerke, the graphitisation has been performed at a temperature of 700 °C. The large amount of silicon, which is used to destabilise the cementite, results in a significantly higher ultimate tensile strength compared to low carbon free-cutting steels [29].

3.2. Tension specimen test under quasi-static and ambient conditions

Axisymmetric smooth and notched tensile specimens are tested with a constant strain rate of $10^{-3}s^{-1}$ at ambient temperature, which is general accepted and commonly used by several researchers [21,17,22,23,30,25,6,5,24,31]. The geometry of the smooth specimens is illustrated in Fig. 3. The initial neck radii of the tested notched specimens are $R = 0.8$, $R = 4$ and $R = 10$mm, as indicated in Fig. 4. The different notch radii permit different levels of hydrostatic tension in the samples during straining [17]. To enable the reproducibility, three samples of each notch radius are manufactured and tested, including the smooth geometry. As shown in Fig. 3 and Fig. 4, the initial diameters of the necking cross-section with a value of 6 mm are kept constant for all specimens and are measured exactly before testing.

To obtain the fracture strain on the basis of Eq. (13) for each specimen from the test data, an average diameter of the necking cross-section is measured using Zoller Venturion 450 measuring machine (E. Zoller GmbH & Co. KG, Germany) after the tests are finished. The fracture strain outlier of one notched specimen with an initial neck radius of 0.8 mm has to be excluded by reason of minimal difference between initial and fracture cross-section diameter. The results of the diameters are listed in Table 1.

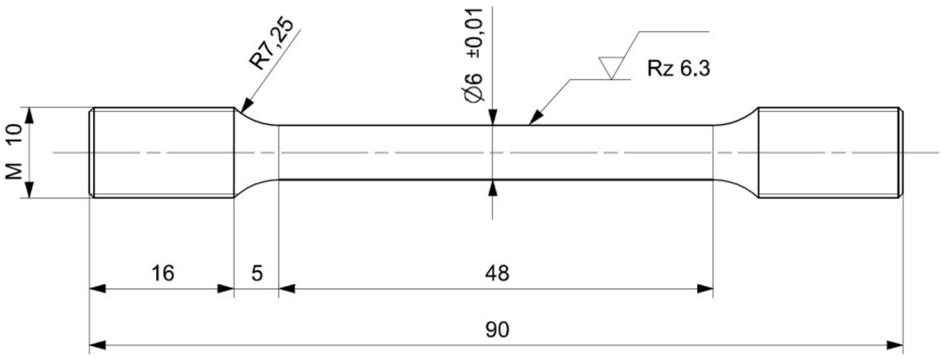

Fig. 3. Smooth tensile specimen.

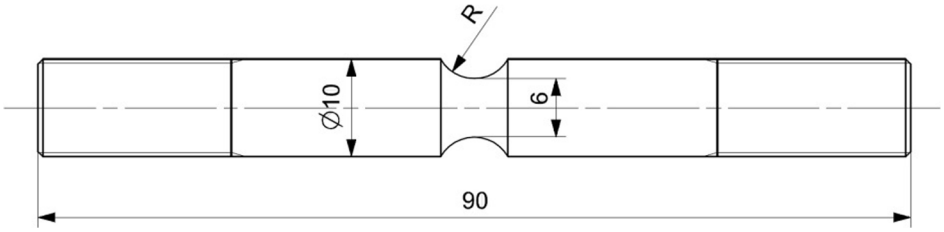

Fig. 4. Notched tensile specimen.

Table 1
Geometrical measurements of the specimens under quasi-static and ambient conditions.

Notch radius 0.8 mm:		
Sample Nr.	**Initial diameter [mm]**	**Average fracture diameter [mm]**
Sample 1	6.00	5.67
Sample 3	6.02	5.67
Notch radius 4 mm:		
Sample Nr.	**Initial diameter [mm]**	**Average fracture diameter [mm]**
Sample 1	6.00	5.19
Sample 2	5.99	5.23
Sample 3	6.00	5.27
Notch radius 10 mm:		
Sample Nr.	**Initial diameter [mm]**	**Average fracture diameter [mm]**
Sample 1	6.01	4.90
Sample 2	5.99	4.90
Sample 3	5.99	4.91
Notch radius ∞ mm (smooth):		
Sample Nr.	**Initial diameter [mm]**	**Average fracture diameter [mm]**
Sample 1	6.00	4.75
Sample 2	5.99	4.66
Sample 3	5.99	4.62

3.3. Tension specimen test under high strain rate and high temperature conditions by Split Hopkinson tension bar (SHTB) test

For understanding the response of material for extreme cases in manufacturing processes, especially machining processes, SHTB tests can be used that facilitate knowing the dynamic stress–strain response of materials at high strain rates and temperatures. More details about the setup of the SHTB tests can be found in literature, i.e. in [32,33]. The details of the specimens are shown in Fig. 5. The specimens used for SHTB tests were prepared by wire-EDM cutting from a steel rod having a diameter of 65 mm. In this study, as shown by Cadoni et al. [34], a semi-conductor strain-gage station is glued on the input bar at 750 mm from the specimen in order to record the deformation of the bar caused by the incident tension pulse during the propagation toward the specimen. A second semi-conductor on the output bar records the deformation caused on the bar by the part of the incident pulse which has been sustained by the specimen. In order to perform high temperature tests, the system is equipped with a water-cooled induction heating system [35]. The thermocouple is welded in the middle part of the gauge length of the sample.

To perform the experiment, initially a hydraulic actuator of maximum loading capacity of 600kN, is pulling part of the input bar (6 m) as pretension bar with a diameter of 10 mm. The pretension stored in this bar is arrested by a blocking device. The rupture of a fragile bolt in the blocking device gives rise to a tensile mechanical pulse of 2.4 ms duration with linear loading rate during the rise time (about 30 μs). Then the load propagates along the input and output bars and fractures the specimen. Images are captured before and after the failure of the specimen, in order to characterise the reduced area of the specimen's cross section and fracture strain.

The list of SHTB tests is given in Table 2. The experiments are performed for five different temperatures starting from room temperature rising in steps of 200 °C up to 800 °C for three levels of strain rates. In order to reduce the number of experiments, not every temperature was combined with every strain rate. The numbers of experiment repetitions are mentioned for each strain rate and temperature in Table 2. The results of the experiments are shown in Table 3. In this work the strain rates above $\dot{\varepsilon} = 500\ s^{-1}$ are termed "high strain rates".

3.4. Parameter identification

All material parameters of the original and modified JC fracture strain equation are optimised and validated for the material 50SiB8 with least squares fit using Levenberg-Marquardt algorithm based on Coleman and Zhang [36] , according to Levenberg [37] and Marquardt [38], and global optimization for each factor in Matlab®, respectively. Eq. (25), according to Coleman and Zhang [36], and Eq. (26) show the commonly used equations for least squares fit and the executed one for the first factor of the original and modified JC fracture strain equation using the forward parameter identification method.

$$\min_x \|F(c, x_{data}) - y_{data}\|_2^2 = \min_x \sum_i (F(c, x_{data\ i}) - y_{data\ i})^2 \tag{25}$$

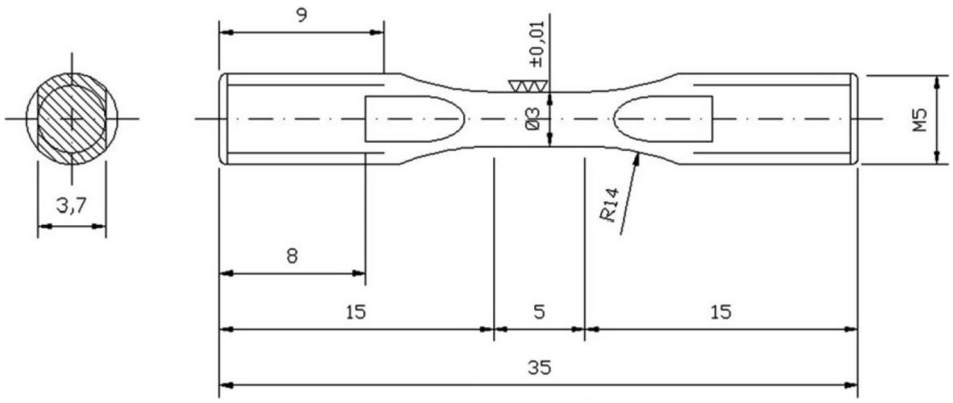

Fig. 5. Specimen geometry for SHTB tests. The location of the output, input strain gages as well as preload strain gages are shown in [35].

Table 2
Overview of the SHTB tests.

Temperature [°C]	Strain-rate [1/s]		
	500	900	1700
20	4	4	4
200	3	3	–
400	3	3	–
600	3	3	–
800	3	3	–

where c, x_{data}, y_{data} are the coefficients, given input data and observed output data, respectively. According to Eq. (25), the mathematical expression for the first factor parameters of the forward parameter identification method is written as

$$\min_{D_k}\left\|\varepsilon_f(D_k,\eta_{data})-\varepsilon_{f(data)}\right\|_2^2=\min_{D_k}\sum_i\left(\varepsilon_f(D_k,\eta_{data_i})-\varepsilon_{f(data)_i}\right)^2 \quad for\ k\ =\ 1,\ 2,\ 3 \tag{26}$$

where D_k is the stress triaxiality dependent parameters in the first factor of the fracture strain equation. The parameters of η_{data} and $\varepsilon_{f(data)}$ are the calculated initial stress triaxiality from the specimen geometry using Eq. (14) and the calculated fracture strain from the area measurements using Eq. (13). Similarly, the material parameters of the second and third factor are computed and identified using the forward and backward parameter identification method.

Referring to [39], a Taylor-series is used for the residual function $r_i(x)$, as shown in Eq. (27), to consider a trust-region model [40] . Thus, a constrained linear least-squares problem is created

$$\frac{1}{2}\|r_i(x)\|_2^2\approx\frac{1}{2}\|r(x_k)+r'(x_k)(x-x_k)\|_2^2 \tag{27}$$

$$min\ \ \frac{1}{2}\|r(x_k)+J(x_k)(x-x_k)\|_2^2 \tag{28}$$

$$\psi(s)=\frac{1}{2}\|r(x_k)+J(x_k)s\|_2^2=\frac{1}{2}\|r(x_k)\|^2+r(x_k)^TJ(x_k)s+\frac{1}{2}s^TJ(x_k)^TJ(x_k)s \tag{29}$$

$$\|x-x_k\|_2\leqslant\Delta_k \tag{30}$$

where $J(x_k)$ is the Jacobian matrix at x_k, Δ_k is defined as trust-region radius, $r(x_k)$ is the residual function at x_k and s is set to $s = x-x_k$. There are two cases for $\|x-x_k\|_2$, as explained in [39]. In the first case, $\|x-x_k\|_2<\Delta_k$, which leads to:

$$\text{grad}\,\psi(s)=J(x_k)^TJ(x_k)s+J(x_k)^Tr(x_k)=0\quad\text{for a stationary point} \tag{31}$$

whereas in the second case $\|x-x_k\|_2=\Delta_k$, which means:

$$\text{grad}\,\psi(s)=J(x_k)^TJ(x_k)s+J(x_k)^Tr(x_k)=-\lambda_k s\quad\text{for}\quad\lambda_k>0 \tag{32}$$

hence, according to Sun and Yuan [40]:

$$(J(x_k)^TJ(x_k)+\lambda_kI)s=-J(x_k)^Tr(x_k) \tag{33}$$

Using the Newton-Method, leads to:

$$x_{k+1}=x_k-\frac{\nabla f(x_k)}{\nabla^2 f(x_k)} \tag{34}$$

$$x_{k+1}=x_k-\frac{J(x_k)^Tr(x_k)}{(J(x_k)^TJ(x_k)+\lambda_kI)} \tag{35}$$

The Levenberg-Marquardt method is characterized by the following equation:

$$(J(x_k)^TJ(x_k)+\lambda_kI)s_K=-J(x_k)^Tr(x_k) \tag{36}$$

according to Sun and Yuan [40]. A global optimum is found by Global Optimization Toolbox solvers, which are designed to search through more than one local minimum [41].

4. Results and discussion

4.1. Results from the forward parameter identification method

Starting with the forward parameter identification method of the original and modified JC fracture strain constitutive equation, the fracture strain – stress triaxiality diagram including the fitted curve of Eq. (15) is shown in Fig. 6. The material parameters D_1, D_2 and $D_3$of the triaxiality-dependent first factor are summarized in Table 4 and Table 5 for the original and modified JC fracture strain constitutive equation, respectively. The residual sum of squares (RSS), according to Kleinbaum [42], is a measurement of discrepancy between the test data, as indicated with black circles, and the estimated model, shown as red curves in the present work. The curve fits in the data points well.

Based on Eq. (16), the fracture strain is plotted as a function of the strain rate for 50SiB8 in Fig. 7 on the left-hand side for the original JC fracture model. It should be noticed that the reference strain rate is set to $\dot{\varepsilon}_0=0.001\,s^{-1}$ for the original JC fracture strain equation. The strain rate range from $500s^{-1}$ to $900s^{-1}$ results in a point cloud due to absent data in the low strain rate field. The fracture strain – strain rate diagram for the modified JC fracture model, as expressed in Eq. (17) with the identified strain rate dependent material parameter, is shown in Fig. 7 on the right-hand side. The reference strain rate is set to $\dot{\varepsilon}_0=1\,s^{-1}$ for the modified JC fracture model. Independent of the original or modified JC fracture model, the limitation can be already seen by computing the strain rate dependent parameter of the second factor. The values of the material parameter D_4 can be found in Table 4 and Table 5 for both JC

Table 3
results of the SHTB tests.

Sample Nr.	Temperature [°C]	Average strain rate [1/s]	Initial diameter [mm]	Average fracture diameter [mm]
Sample 1	20	1757	3.00	2.05
Sample 2	20	1617	3.01	2.05
Sample 3	20	1642	3.00	2.04
Sample 4	20	907	3.01	2.07
Sample 5	20	478	3.01	2.08
Sample 6	400	938	3.00	1.95
Sample 7	400	510	3.01	2.00
Sample 8	800	921	3.00	1.40
Sample 9	800	471	3.00	1.40
Sample 10	200	885	3.00	2.00
Sample 11	200	454	3.01	2.05
Sample 12	600	747	3.01	2.20
Sample 13	600	476	3.00	2.00
Sample 14	400	954	3.00	1.85
Sample 15	400	954	3.00	1.90
Sample 16	400	504	3.00	1.90
Sample 17	400	509	3.00	1.90
Sample 18	800	897	3.00	1.35
Sample 19	800	893	3.01	1.30
Sample 20	800	444	3.00	1.30
Sample 21	800	448	3.00	1.25
Sample 22	20	889	3.00	2.10
Sample 23	20	887	3.00	2.05
Sample 24	20	491	3.01	2.00
Sample 25	20	472	3.01	2.10
Sample 26	20	484	3.01	2.10
Sample 27	20	894	3.01	2.10
Sample 28	20	1678	3.01	2.00
Sample 29	200	464	3.00	2.00
Sample 30	200	463	3.03	2.00
Sample 31	200	898	3.00	2.00
Sample 32	200	876	3.00	2.00
Sample 33	600	468	3.00	2.00
Sample 34	600	446	3.00	2.00
Sample 35	600	924	3.00	2.00
Sample 36	600	919	3.00	2.00

fracture models.

For the identification of the temperature dependent material parameters, each specified strain rate from around $500s^{-1}$ to $900s^{-1}$ is taken into account. Since Eq. (18) is used for both JC fracture models, the fracture strain – temperature diagram with the curve fitted function for the strain rate of $700s^{-1}$ looks the same for the original and modified JC fracture model and is shown in Fig. 8. A nonlinear relation between

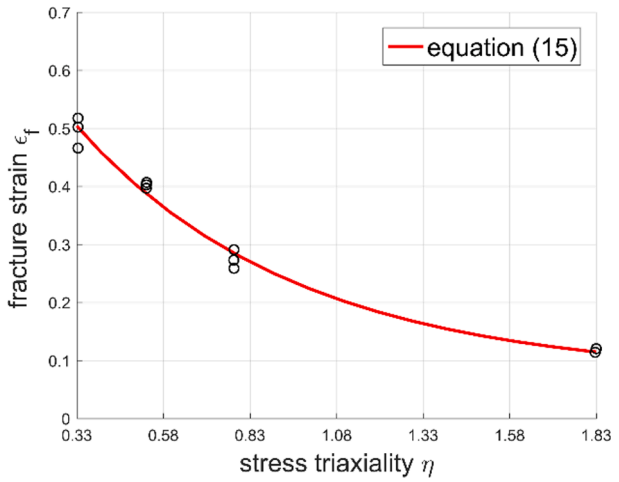

Fig. 6. Identification of the stress triaxiality dependent parameters D_1, D_2 and D_3 for the original and modified JC fracture strain model using the forward parameter identification method.

Table 4
Material parameters of the original Johnson-Cook fracture equation for 50SiB8.

	D_1	D_2	D_3	D_4	D_5
Forward parameter identification	0.0733	0.7204	−1.5643	0.0371	1.5583
Backward parameter identification	0.1138	0.3973	−1.1127	0.0692	1.5723

Table 5
Material parameters of the modified Johnson-Cook fracture equation for 50SiB8.

	D_1	D_2	D_3	D_4	D_5
Forward parameter identification	0.0733	0.7204	−1.5643	0.0602	1.6157
Backward parameter identification	0.1138	1.0958	−2.4907	0.0360	1.5743

fracture strain and temperature is clearly noticeable. The functional dependence on temperature in the JC-fracture strain equations is obviously not sufficient for the analysed free-cutting steel due to a blue-brittle reduction of fracture strain as temperature reaches 600 °C. A proposal for the blue-brittle and temperature factor is given in Section 4.4. The similar temperature dependent parameters D_5 can be found in Table 4 and Table 5 for the original and modified JC fracture model, respectively.

4.2. Results from the backward parameter identification method

In case of the backward parameter identification, the curves, based on Eqs. (19) and (20), are shown in Fig. 9 on the left- and right-hand side for the original and modified JC fracture model, respectively. The corresponding identified parameters are $\varepsilon_{f_0} = 0.3880$ for the original version and $\varepsilon_{f_0} = 0.5916$ for the modified JC fracture model. As already mentioned, the absent data points in the low strain rate field have an obviously influence on the curve. It should be noticed that the reference strain rate is $\dot{\varepsilon}_0 = 0.001\,s^{-1}$ for the original JC fracture model and $\dot{\varepsilon}_0 = 1\,s^{-1}$ for the modified version. The strain rate dependent parameter D_4 can be found in Table 4 and Table 5 for the original and modified version of the JC fracture model, determined by the backward parameter identification method.

The identification of the temperature dependent material parameter D_5 using the backward method and the corresponding curve fitting Eqs.

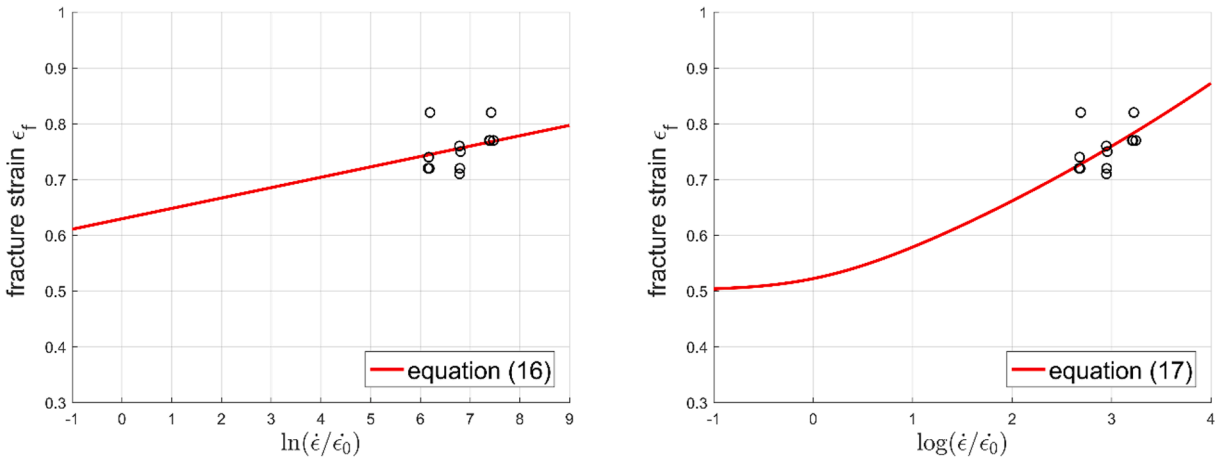

Fig. 7. Identification of the strain rate dependent parameter D_4 for the original (left) and the modified (right) JC fracture model using the forward parameter identification method.

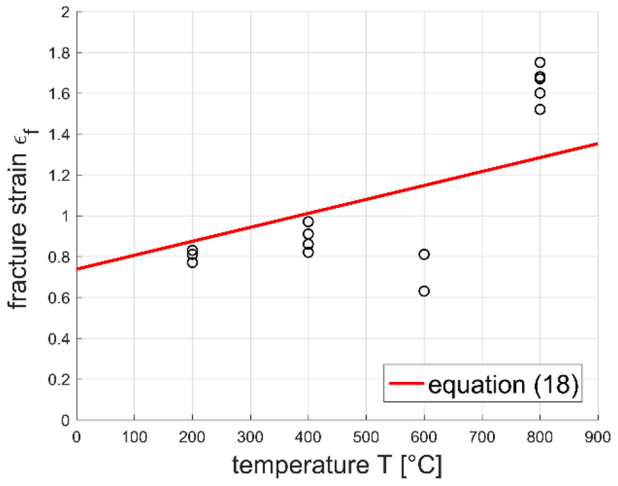

Fig. 8. Identification of the temperature dependent parameter D_5 for the original and modified JC fracture model using the forward parameter identification method.

(21) and (22) with an exemplary strain rate of $700s^{-1}$ is illustrated in Fig. 10 for the original and modified version of the JC fracture model. The temperature parameter is shown in Table 4 and Table 5 for the original and modified version, in which each specified strain rate from $500s^{-1}$ to $900s^{-1}$ is taken into account, as already above-mentioned for the forward parameter identification method. The nonlinear behaviour between fracture strain and temperature cannot be neglected. The linear temperature functions from both JC fracture models do not represent the behaviour of 50SiB8 steel through the analysed temperature range at all due to blue-brittle reduction of fracture strain as temperature reaches 600 °C. As above-mentioned, a proposal for the blue-brittle and temperature factor is given in Section 4.4.

To identify the first factor parameters of the original and modified JC fracture strain equation using the backward parameter identification method and the corresponding Eqs. (23) and (24), a few assumptions for the material parameters have to be considered. According to Børvik et al. [25], the value of the parameter D_1 should not be lower than the calculated data points and the fitted curve has to pass through the already identified quasi-static fracture strain data point $\varepsilon_{f_0} = 0.3880$ for the original and $\varepsilon_{f_0} = 0.5916$ for the modified JC facture model, which are marked as black squares in Fig. 11. Based on those supporting points, the data points of the smooth specimens are not included. A qualitative difference can be observed between the original (left image of Fig. 11) and the modified (right image of Fig. 11) first factor of the JC fracture model, obtained with the backward parameter identification method. The quantified values are shown in Table 4 and Table 5 for the original and modified version, respectively.

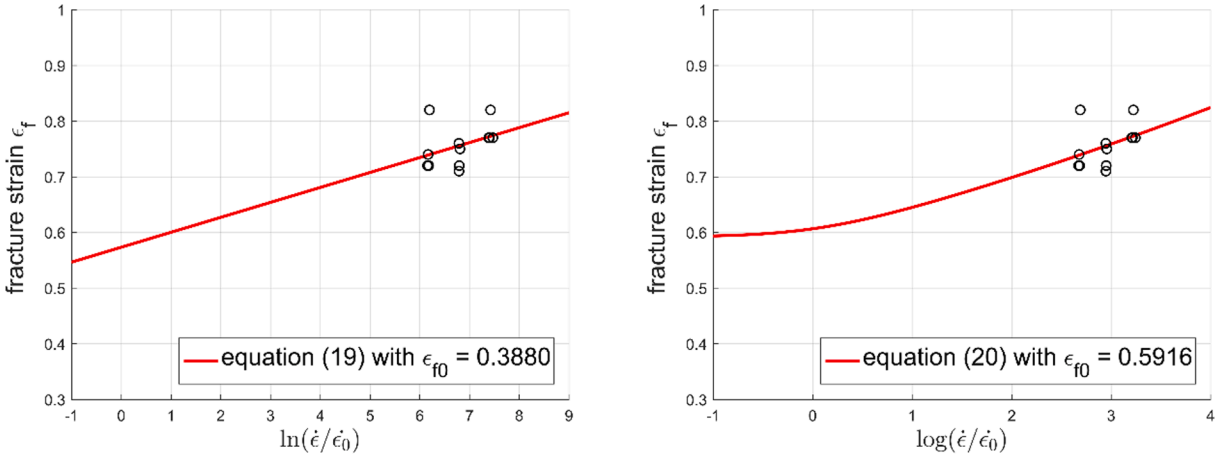

Fig. 9. Identification of D_4 and ε_{f_0} for the original (left) and modified (right) JC fracture strain equation using the backward parameter identification method.

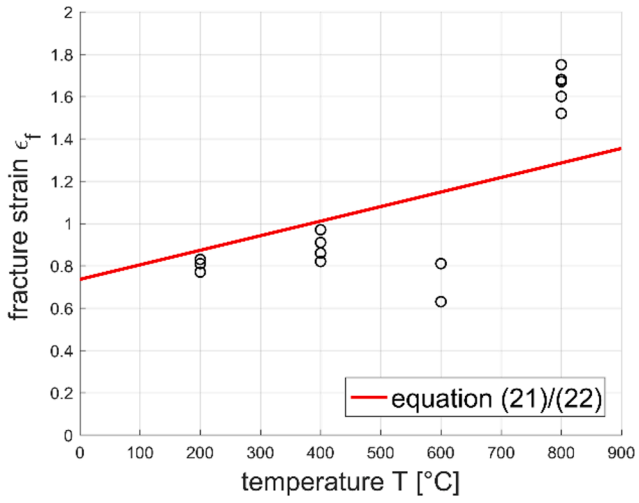

Fig. 10. Identification of temperature dependent parameter D_5 for the original and modified JC fracture strain equation using the backward parameter identification method.

4.3. Comparing forward and back parameter identification method

The material parameters for two different fracture strain constitutive equations, the original and slightly modified JC models, are identified in the previous two sub-chapters. The forward and backward parameter identification method are used for both, the original and slightly modified, JC fracture strain equations, indicating different values for the material parameters for free-cutting steel 50SiB8 with graphite inclusion. The results of the material parameter identification for the original and modified JC fracture strain equation are summarised in Table 4 and Table 5, respectively.

In the case of the stress triaxiality dependent factor with the parameters D_1, D_2 and D_3, the forward parameter identification method (FPIM) is preferred for the original JC constitutive equation, as clearly shown in Fig. 12 with a lower RSS-value. By contrast, the backward parameter identification method (BPIM) should be implemented for the modified JC fracture equation, as seen in Fig. 13. Comparing the second factors and also the third factors to each other, the RSS-values are quite similar in each case.

4.4. Blue-brittleness behaviour of free-cutting steel 50SiB8

Irrespective of the parameter identification method, all temperature tests of 50SiB8 indicate a non-linear relation between fracture strain and

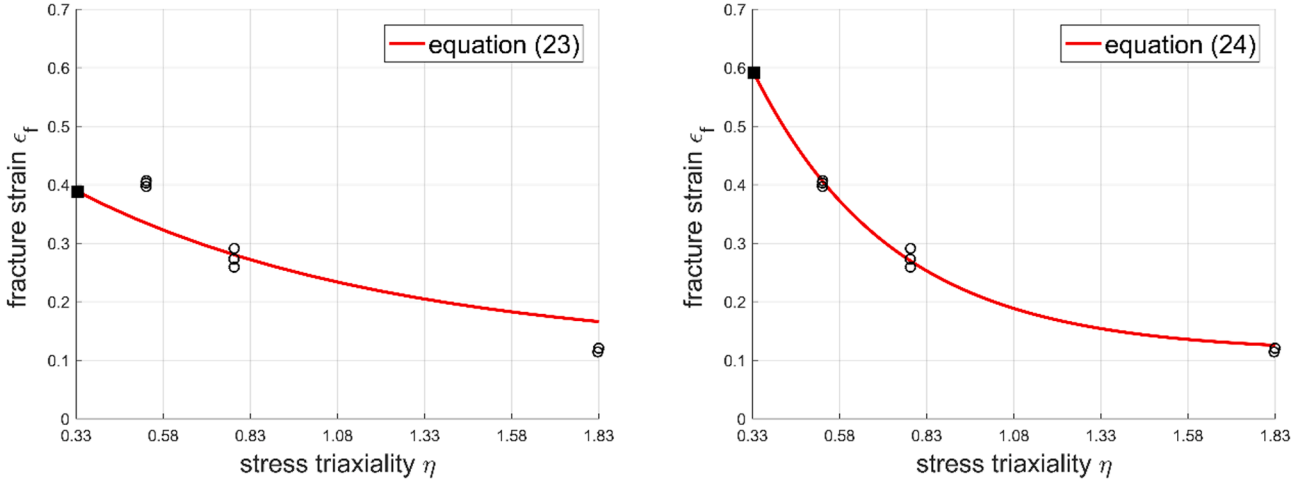

Fig. 11. Identification of the stress triaxiality dependent parametersD_1, D_2 and D_3 for the original (left) and modified (right) JC using the backward parameter identification method.

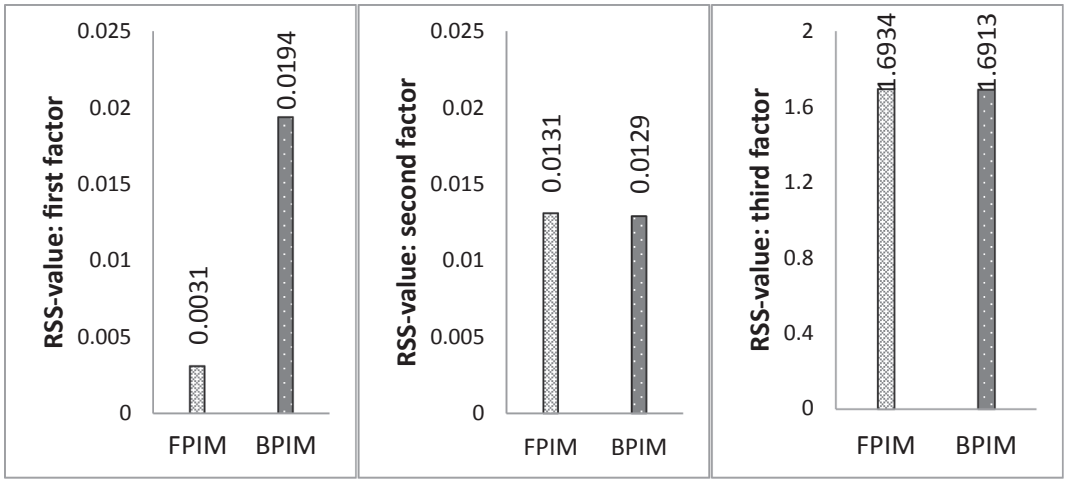

Fig. 12. RSS-value comparison of the three factors using the original JC fracture strain equation.

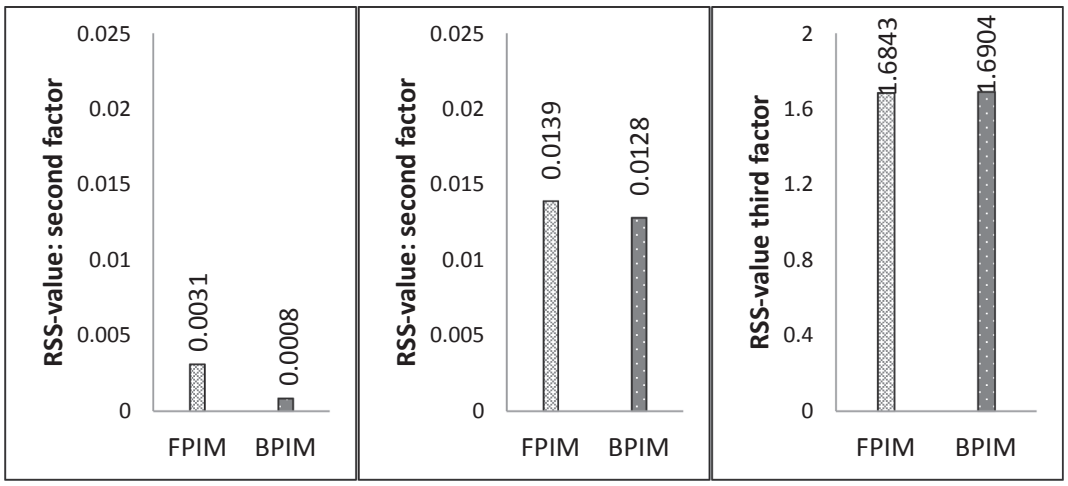

Fig. 13. RSS-value comparison of the three factors using the modified Johnson-Cook fracture strain equation.

temperature for both JC equations. The temperature data indicate a typical behaviour of carbon steels, which is a drop of ductility and leads to a blue-brittle reduction of fracture strain as temperature reaches 600 °C, in conjunction with high strain rates. Blue-brittleness is an effect of dynamic strain aging and needs to be taken into account if the material in the cutting process is heated up in or through this temperature region. Hence, the temperature factor of both fracture strain constitutive equations, the original and slightly modified JC model, are adjusted to a fourth-degree polynomial function including the blue brittle effect for high strain rates, as shown in Eqs. (37) and (38), respectively:

$$\varepsilon_f = \left[D_1 + D_2\, e^{D_3\,\eta}\right]\left[1 + D_4\, ln\left(\frac{\dot{\varepsilon}}{\dot{\varepsilon}_0}\right)\right]\left[1 + D_5\, T^* + D_6 (T^*)^2 + D_7 (T^*)^3 + D_8 (T^*)^4\right] \tag{37}$$

and for the modified JC equation:

$$\varepsilon_f = \left[D_1 + D_2\, e^{D_3\,\eta}\right]\left[1 + \dot{\varepsilon}^*\right]^{D_4}\left[1 + D_5 T^* + D_6 (T^*)^2 + D_7 (T^*)^3 + D_8 (T^*)^4\right] \tag{38}$$

The corresponding graphs for the adjusted temperature factors of the original and slightly modified JC fracture strain constitutive equation are illustrated for a strain rate of $700s^{-1}$ in Fig. 14. Each strain rate from around $500s^{-1}$ to $900s^{-1}$ is taken into account. The SHTB tests at high strain rates and room temperature, which are not used for the identification of the temperature dependent material parameters, are included to show that the fit seems reasonable, as similar explained in [25] just for D_5. Those test data are marked blue in Fig. 14. The values of the temperature and blue-brittle dependent material parameters, in case of high strain rates, are summarised in Table 6. The corresponding RSS values for the new adjusted temperature factors are shown in Fig. 15. Using the preferred parameter identification method, the RSS-values have been reduced more than seventeen times for the temperature factor of the original and modified JC equation. Childs [20] has proposed a model with a cubic polynomial function combined with a step function for T ≥ 650 °C, due to insufficient temperature range from 20 to 500 °C, where ε_f gets infinity, based on torsional Hopkinson bar experiments (strain-rate ≈2000 s^{-1}) of a 0.12C re-sulphurized steel, as reported in [43]. Due to an extended temperature range used for the experimental observations in case of the SHBT, the blue brittle dependent model in this study is more accurate. Generally, the dynamic strain aging phenomenon is greatly influenced by the test temperature and the strain rate. Since only the influence of high strain rates at various temperatures are considered in this study (especially for machining simulations),

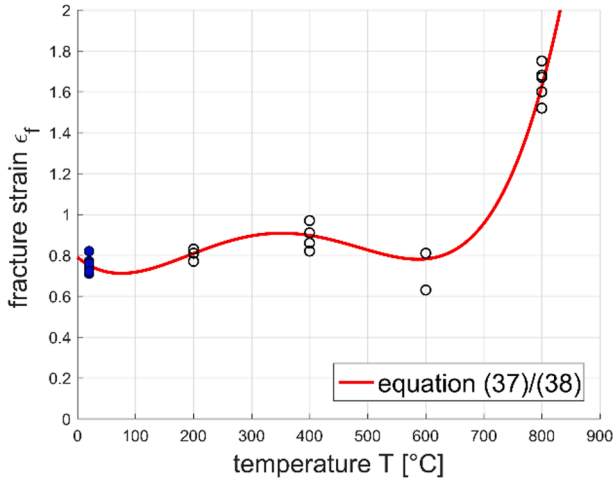

Fig. 14. Identification of the new temperature and blue-brittleness dependent parameters for the original and modified JC fracture strain equation using the forward parameter identification method. (For interpretation of the references to colour in this figure legend, the reader is referred to the web version of this article.)

Table 6
New temperature and blue-brittle dependent material parameters for 50SiB8.

Temperature and blue-brittle dependent parameters:	D_5	D_6	D_7	D_8
Orig. JC forward parameter identification	−3.5642	69.5723	−318.5630	428.9243
Modi. JC backward parameter identification	−3.4807	69.0096	−317.1813	427.9013

additional tests under quasi-static and intermediate strain rates at various temperatures are needed, to fully cover the blue-brittle behaviour of free-cutting steel 50SiB8.

4.5. Numerical analysis

The proposed fracture strain model is validated here within a numerical simulation model of the SHTB test specimen (Fig. 5). The FE-package Abaqus 6.14–1 was used for the simulations and the explicit solver was used since element deletion upon damage is not supported in the implicit Abaqus/Standard solver. The FE model as well as material

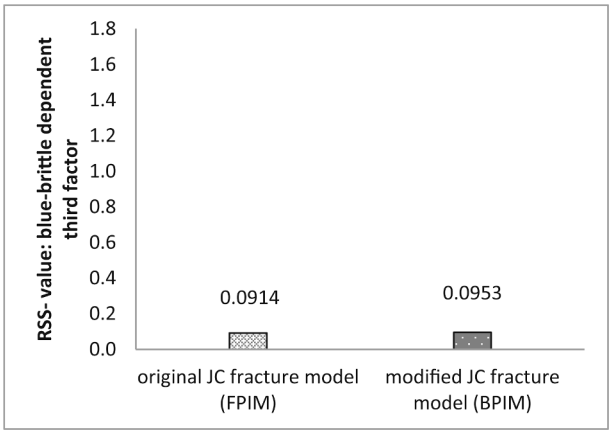

Fig. 15. RSS-values of the new third factors for the original and modified JC fracture strain equation, including blue-brittleness effect.

parameters for 50SiB8 were taken from Klippel et al. [44], who used exactly the same SHTB and tensile tests experiments to deduce the material parameters for a Johnson-Cook flow stress model. This simulation model was extended here with the original JC and the new blue-brittleness dependent fracture strain model, expressed in Eqs. (11) and (37), to compare with each other and with the experimental data. The material parameters of the two fracture strain models, which have been used for simulations, are summarized in Table 8. The geometry and the FE mesh are shown in Fig. 16. The mesh consists of 14,032 elements (types C3D6R and C3D8R) with 16,154 nodes. Left and right to the specimen, time dependent displacements were applied in order to model tensile loading at certain constant strain rates. The regions of boundary condition application are shown in Fig. 17.

Damage accumulation was considered during the loading according to:

$$D = \sum \frac{\Delta \varepsilon_{pl}}{\varepsilon_f} \tag{39}$$

where $\Delta\varepsilon_{pl}$ is the current plastic strain increment and ε_f is the current fracture strain. $D = 0$ is the undamaged state and upon reaching $D = 1$ the corresponding element is deleted. The influence of the damage variable on the yield stress is not considered. After complete rupture of the cross-section, the fracture strain and the fracture diameter are evaluated and compared against the experimental data, as illustrated in Table 9. For the quasi-static tests mass scaling was used to keep the runtimes at a reasonable level. The original JC and the blue-brittle dependent fracture strain models were implemented into a Fortran user subroutine VUMAT. In the simulations, physical constants from Smolenicki [45] and Johnson-Cook flow stress model coefficients from Klippel et al. [44] were used, as provided with Table 7.

In order to simulate adiabatic heating due to plastic dissipation, a Taylor-Quinney coefficient $\eta_{TQ} = 0.9$ was used:

$$\Delta T = \frac{\eta_{TQ} \cdot \sigma_Y}{\rho \cdot c_p} \Delta \varepsilon_{pl} \tag{40}$$

where ΔT is the temperature increase due to plastic dissipation, ρ the density, c_p the specific isobaric heat capacity, σ_Y the current yield stress and $\Delta\varepsilon_{pl}$ the current plastic strain increment. Since adiabatic heating can lead to a significant temperature increase, the temperature part of the new proposed blue-brittle dependent fracture strain equation was limited to a maximum of 2.5 (maximum value of the temperature factor at melting temperature, based on the original JC fracture model in Eq. (11)):

$$max([1 + D_5 T^* + D_6 (T^*)^2 + D_7 (T^*)^3 + D_8 (T^*)^4]; 2.5) \tag{41}$$

This limit was set to avoid unrealistically large fracture strains for temperatures beyond T = 800 °C. This is in contrast to Childs [20], where the fracture strain can reach infinite values beyond temperatures of 650 °C. This behaviour is not considered to be useful in this kind of simulations performed here, as fracture becomes almost impossible beyond certain temperatures. However, in future investigations testing at even higher temperatures should be investigated to gain reliable information about fracture strains towards melting temperature.

A selection of test cases were numerically simulated and the fracture strain and fracture diameter were compared against the experimental tests. The fracture strain from the numerical simulation was taken from the first integration point at failure ($D = 1$), the fracture diameter was averaged from the circumferential nodes left and right from the fracture surfaces, as shown in Fig. 18. The experimental results, as well as the numerical results for the classic and the new model are summarized in Table 9. Both models reasonably predict fracture strains and diameters until T = 400 °C, where the new blue-brittle dependent model shows a tendency to slightly over-predict the fracture diameter, corresponding to smaller fracture strains. Beyond T = 400 °C the original JC model fails to correctly predict the fracture strain and diameter while the newly proposed blue-brittle dependent model performs well and in line with experimental results. A comparison of experimental and numerical predicted (blue-brittle dependent JC) SHTB specimen shapes after rupture at a strain rate of 900/s and different temperatures is provided with Fig. 19. A good qualitative agreement can be seen between the shapes.

4.6. Proposed new fracture model

As detailed described in the introduction, several researchers have also shown that the Lode angle affects widely the stress triaxiality dependent first factor of the JC fracture strain constitutive equation. For that reason, the Bai-Wierzbicki asymmetric fracture locus model with lode angle dependency [6] is combined with the Johnson and Cook fracture strain equation, as stated below in the form of the first factor. In future research, the offset parameter from the first factor of the JC fracture strain equation has also to be considered to plot the fracture surface correctly and identify the material parameters in a more accurate way.

Due to insufficient experimental data in the lower strain rate region (below 500 s^{-1}), a recommendation for the changed second factor of the modified JC fracture strain equation is not applied. For this reason, both, the original and modified JC fracture strain equation are used as basis for the proposed fracture strain constitutive equation, as listed below. The fourth-degree polynomial function is used for the temperature dependent factors with blue-brittleness effect, as already above-

Table 7
Physical constants and JC flow stress coefficients, according to Smolenicki [45] and Klippel et al. [44]

A [MPa]	B [MPa]	C [-]	m [-]	n [-]	$\dot{\varepsilon}_{pl}^0$ [/s]	T_{ref} [K]	T_{melt} [K]	ρ [kg/m^3]	**E [GPa]**	**ν [-]**	η_{TQ} **[-]**	c_p **[J/(kgK)]**
430.9	908.7	0.00447	0.7361	0.3854	0.001	293.15	2006	7850	214	0.334875	0.90	466

Table 8
Material parameters for the original (top) and blue-brittle dependent JC fracture strain equation.

Fracture strain model	Eq.	D_1 [-]	D_2 [-]	D_3 [-]	D_4 [-]	D_5 [-]	D_6 [-]	D_7 [-]	D_8 [-]
JC classic	(11)	0.0733	0.7204	−1.5643	0.0371	1.5583	–	–	–
JC blue-brittle	(37)	0.0733	0.7204	−1.5643	0.0371	−3.5642	69.5723	−318.5630	428.9243

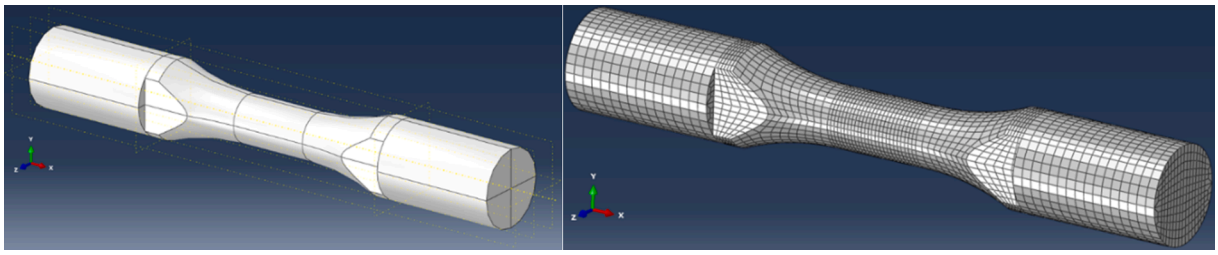

Fig. 16. Geometry (left) and mesh (right) of the SHTB test specimen, from Klippel et al. [44]

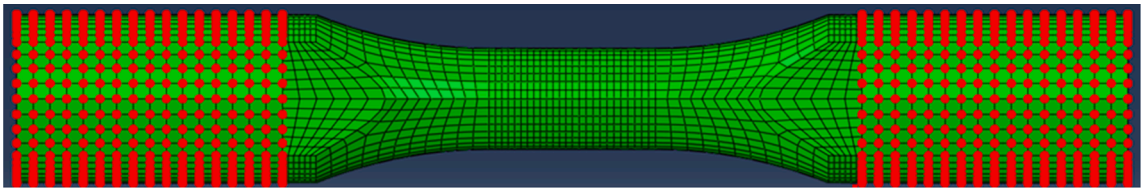

Fig. 17. Displacement boundary condition application at nodes (marked in red) on the left and right side of the specimen. (For interpretation of the references to colour in this figure legend, the reader is referred to the web version of this article.)

Table 9
Simulated test cases and comparison to experimental values.

Initial Conditions		Experimental results				original JC model		New blue-brittle model	
Test temperature [°C]	Strain rate simulation[1/s]	Average strain rate experiments [1/s]	Initial Diameter $Ø_f$ [mm]	FractureStrain ε_f [%]	Fracture Diameter $Ø_f$ [mm]	Strain ε_f [%]	Diameter $Ø_f$ [mm]	Strain ε_f [%]	Diameter $Ø_f$ [mm]
20	0.001	0.001	5.99–6.00	46.7–51.9	4.62–4.75	50.2	4.64	46.6	4.73
20	500	472–491	3.01	72.0–81.8	2.00–2.10	70.5	2.08	65.1	2.15
20	900	887–907	3.00–3.01	71.3–76.2	2.05–2.10	71.6	2.07	66.1	2.13
20	1700	1617–1757	3.00–3.01	76.2–81.8	2.00–2.05	72.9	2.05	67.3	2.11
200	900	876–898	3.00	81.1	2.00	81.4	1.96	77.4	2.01
400	900	938–954	3.00	86.2–96.7	1.85–1.95	91.3	1.86	76.4	2.02
600	900	747–924	3.00–3.01	62.7–81.1	2.00–2.20	100.6	1.76	76.1	2.02
800	900	893–921	3.00–3.01	152–168	1.30–1.40	109.4	1.67	140.5	1.36

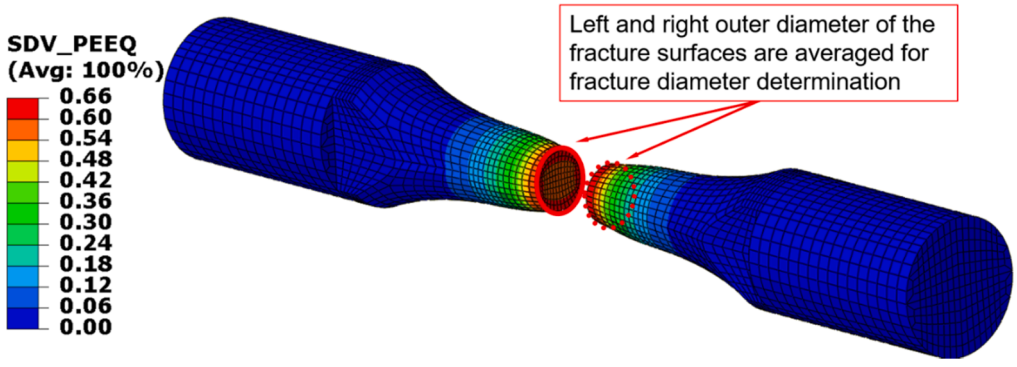

Fig. 18. Plastic strain distribution after rupture of a SHTB test specimen at T = 20 °C and a strain rate of 900/s. Left and right fracture surfaces show encircled the nodes from which the averaged fracture diameter was determined.

T [°C]	Picture of fractured specimen [44]	Numerical prediction of the distribution of the damage variable D with the blue-brittle dependent JC fracture strain model after fracture has occured: elements coloured in blue relate to undamaged material (D=0) and orange/red elements are close to fracture (D<1), fully damaged elements (D=1) are deleted and not displayed
20	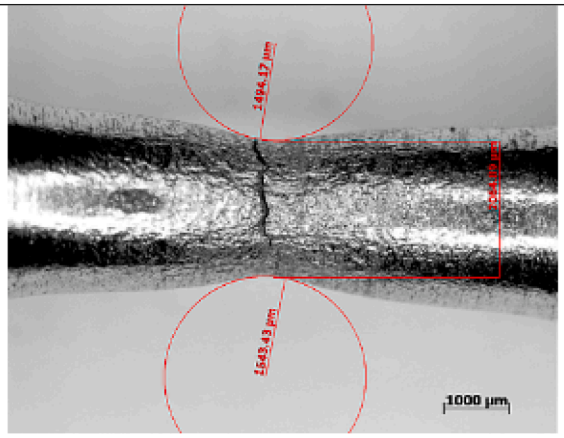	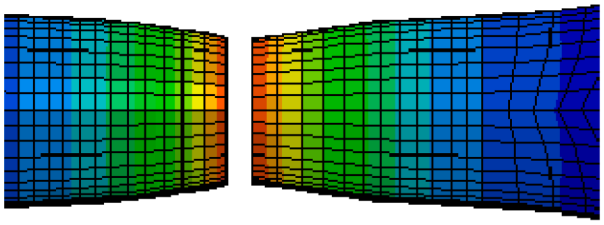
400	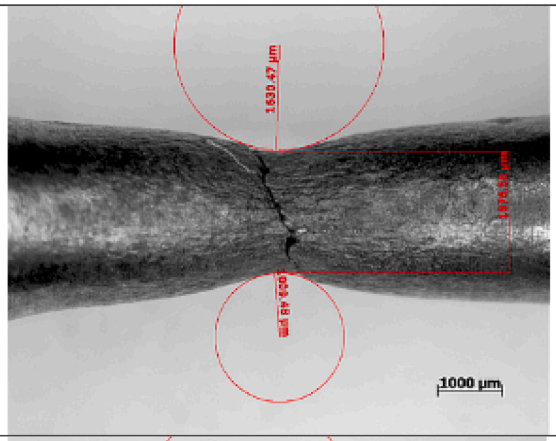	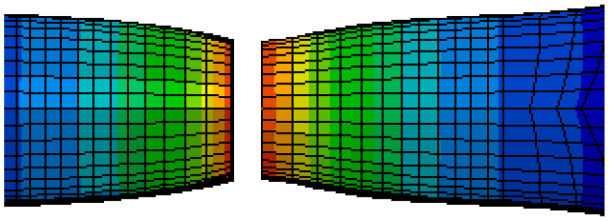
800	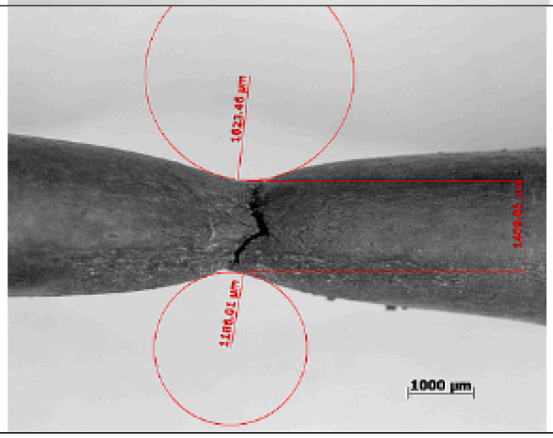	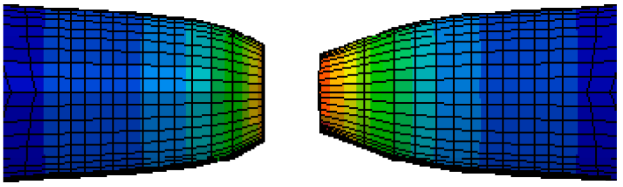

Fig. 19. Comparison of experimental (middle column) versus simulated (right column) fracture at a strain rate of 900/s for different temperatures: top at T = 20 °C, middle: T = 400 °C, bottom: T = 800 °C.

mentioned. The mathematical expression of the new recommended fracture strain constitutive equation, using the second factor of the original Johnson and Cook, based on Eq. (11), is written as:

$$\varepsilon_f = \left[\left(\frac{1}{2}\left(D_{1tr}\, e^{-D_{2tr}\,\eta} + D_{5tr}\, e^{-D_{6tr}\,\eta}\right) - D_{3tr}\, e^{-D_{4tri}\,\eta}\right)\overline{\theta}^2 + \right.$$

$$\left. + \frac{1}{2}\left(D_{1tr}\, e^{-D_{2tr}\,\eta} - D_{5tr}\, e^{-D_{6tr}\,\eta}\right)\overline{\theta} + D_{3tr}\, e^{-D_{4tr}\,\eta}\right]\left[1 + \; D_{7st}\, ln\left(\frac{\dot{\varepsilon}}{\dot{\varepsilon}_0}\right)\right]\cdot\cdot\left[1 \right.$$

$$\left. + D_{8T}\, T^* + D_{9T}\,(T^*)^2 + D_{10T}\,(T^*)^3 + D_{11T}\,(T^*)^4\right] \tag{42}$$

and, using the second factor of the modified JC fracture strain function, based on Eq. (12), the proposing fracture strain equation is:

$$\varepsilon_f = \left[\left(\frac{1}{2}\left(D_{1tr}\, e^{-D_{2tr}\,\eta} + D_{5tr}\, e^{-D_{6tr}\,\eta}\right) - D_{3tr}\, e^{-D_{4tri}\,\eta}\right)\overline{\theta}^2 + \right.$$

$$\left. + \frac{1}{2}\left(D_{1tr}\, e^{-D_{2tr}\,\eta} - D_{5tr}\, e^{-D_{6tr}\,\eta}\right)\overline{\theta} + D_{3tr}\, e^{-D_{4tr}\,\eta}\right]\left[1 + \; \frac{\dot{\varepsilon}}{\dot{\varepsilon}_0}\right]^{D_{7st}}\cdot\cdot\left[1 + D_{8T}\, T^* \right.$$

$$\left. + D_{9T}\,(T^*)^2 + D_{10T}\,(T^*)^3 + D_{11T}\,(T^*)^4\right] \tag{43}$$

In future research, the parameters of these new suggested fracture models should be calculated and implemented in simulation of processes i.e. nonlinear finite element or element free methods.

5. Conclusion

Material parameters of free-cutting steel 50SiB8 for the original and modified JC fracture strain constitutive equation are determined in this paper. The SHTB and tension experiments are performed under quasi-static, isothermal, high temperature and high strain rate conditions using smooth and notched tension specimens. Each of the experiments is performed at least three times. Two different parameter identification methods are used for each JC fracture strain equation to analyse the wide influence on the material parameters and to compare explicitly the residual sum of squares (RSS) values. Based on these RSS-values, a recommendation for each fracture strain equation is given.

According to the RSS-values and focusing the stress triaxiality factor, the forward parameter identification method is recommended for the original JC fracture strain equation. In the case of the modified JC fracture strain equation, the backward parameter identification procedure is approved. A recommendation for enhancing the strain rate factor is not possible.

Tests at elevated temperature for 50SiB8 indicate a clearly non-linear relation between fracture strain and temperature, which is attributed to the blue-brittleness effect in those steels. This leads to a fourth-degree polynomial function for the temperature and blue-brittle dependent factors of both original and modified JC fracture strain equations. Using the preferred parameter identification method, the temperature material parameters which are influenced by blue brittleness, have also been determined for the new factor. The fourth-degree polynomial function reduces the RSS-values of the temperature and blue-brittle factors more than seventeen times for the original and modified JC fracture equation. Since only the influence of high strain rates at various temperatures are considered in this study (especially for machining simulations), additional tests under quasi-static and intermediate strain rates at various temperatures are suggested, to fully cover the blue-brittle behaviour of free-cutting steel 50SiB8.

FE simulations were carried out once with the classical Johnson-Cook fracture strain equation and once for the new blue-brittle adjusted Johnson-Cook fracture strain equation. Fracture strain and fracture diameter were evaluated and compared against the experimental SHTB data. Both models reasonably predict fracture strains and diameters until T = 400 °C. Beyond T = 400 °C the classical JC model fails to correctly predict the fracture strain and diameter while the newly proposed model including the blue-brittleness effect fits well with the experimental results. Although the numerical analysis with the proposed temperature and blue-brittle dependent parameters of 50SiB8 can adequately validate the experimental data, it may be not applicable under quasi-static and intermediate strain rate conditions. Further experimental investigations in the last-mentioned strain rate range are suggested. However, in case of machining simulations with high strain rates and temperature values, the blue-brittleness effect for free-cutting steel 50SiB8 is examined extensively.

Taking also the stress triaxiality with the Lode angle in conjunction with the Bai-Wierzbicki asymmetric fracture locus model for the first factor and the blue-brittle dependent factor of both JC equations into account, two new recommended fracture strain constitutive equations have been proposed.

CRediT authorship contribution statement

Marcel Gerstgrasser: Conceptualization, Methodology, Formal analysis, Investigation, Data curation, Writing - original draft, Visualization. **Darko Smolenicki:** Conceptualization, Investigation, Data curation. **Mansur Akbari:** Conceptualization, Project administration. **Hagen Klippel:** Methodology, Software, Validation, Writing - original draft, Visualization. **Hans Roelofs:** Investigation, Resources. **Ezio Cadoni:** Investigation, Writing - review & editing. **Konrad Wegener:** Supervision, Writing - review & editing.

Declaration of Competing Interest

The authors declare that they have no known competing financial interests or personal relationships that could have appeared to influence the work reported in this paper.

Acknowledgements

The authors would like to thank the Swiss National Science Foundation for the financial support under the number 200021-117847, Swiss Innovation Agency Innosuisse for financial support in the frame of project 13983.2 PFIW-IW, Mr. Andreas Zschippang and Mr. Roland Pauli.

References

[1] F.A. McClintock, A criterion for ductile fracture by the growth of holes, J. Appl. Mech. 35 (1968) 363–371.
[2] J.R. Rice, D.M. Tracey, On the ductile enlargement of voids in triaxial stress fields*, J. Mech. Phys. Solids 17 (1969) 201–217.
[3] A.C. Mackenzie, J.W. Hancock, D.K. Brown, On the influence of state of stress on ductile failure initiation in high strength steels, Eng. Fract. Mech. 9 (1977) 167–188.
[4] G.R. Johnson, W.H. Cook, Fracture characteristics of three metals subjected to various strains, strain rates, temperatures and pressures, Eng. Fract. Mech. 21 (1985) 31–48.
[5] Y. Bai, X. Teng, T. Wierzbicki, On the application of stress triaxiality formula for plane strain fracture testing, J. Eng. Mater. Technol. 131 (2009), 021002.
[6] Y. Bai, T. Wierzbicki, A new model of metal plasticity and fracture with pressure and Lode dependence, Int. J. Plast. 24 (2008) 1071–1096.
[7] W. Lode, Versuche über den Einfluß der mittleren Hauptspannung auf das Fließen der Metalle Eisen, Kupfer und Nickel. Zeitschrift für Physik. 36 (1926) 913–939.
[8] M. Luo, M. Dunand, D. Mohr, Experiments and modeling of anisotropic aluminum extrusions under multi-axial loading – Part II: Ductile fracture, Int. J. Plast. 32 (2012) 36–58.
[9] M. Brünig, S. Gerke, V. Hagenbrock, Stress-state-dependence of damage strain rate tensors caused by growth and coalescence of micro-defects, Int. J. Plast. 63 (2014) 49–63.
[10] L. Malcher, E.N. Mamiya, An improved damage evolution law based on continuum damage mechanics and its dependence on both stress triaxiality and the third invariant, Int. J. Plast. 56 (2014) 232–261.

[11] C.C. Roth, D. Mohr, Effect of strain rate on ductile fracture initiation in advanced high strength steel sheets: Experiments and modeling, Int. J. Plast. 56 (2014) 19–44.
[12] S.J. Marcadet, D. Mohr, Effect of compression–tension loading reversal on the strain to fracture of dual phase steel sheets, Int. J. Plast. 72 (2015) 21–43.
[13] C.C. Roth, D. Mohr, Ductile fracture experiments with locally proportional loading histories, Int. J. Plast. 79 (2016) 328–354.
[14] N.S. Ottosen, M. Ristinmaa, The mechanics of constitutive modeling, Elsevier (2005).
[15] S. Buchkremer, J. Schoop, A mechanics-based predictive model for chip breaking in metal machining and its validation, CIRP Annals – Manufact. Technol. 65 (2016) 69–72.
[16] A.S. Khan, H. Liu, Strain rate and temperature dependent fracture criteria for isotropic and anisotropic metals, Int. J. Plast. 37 (2012) 1–15.
[17] T. Børvik, O. Hopperstad, T. Berstad, M. Langseth, A computational model of viscoplasticity and ductile damage for impact and penetration, European J. Mech.-A/Solids. 20 (2001) 685–712.
[18] Y. Bai, T. Wierzbicki, A comparative study of three groups of ductile fracture loci in the 3D space, Eng. Fract. Mech. 135 (2015) 147–167.
[19] S. Buchkremer, F. Klocke, D. Veselovac, 3D FEM simulation of chip breakage in metal cutting, Int. J. Adv. Manufact. Technol. 82 (2016) 645–661.
[20] T. Childs, Ductile shear failure damage modelling and predicting built-up edge in steel machining, J. Mater. Process. Technol. 213 (2013) 1954–1969.
[21] T. Børvik, M. Langseth, O. Hopperstad, K. Malo, Ballistic penetration of steel plates, Int. J. Impact Eng. 22 (1999) 855–886.
[22] A.H. Clausen, T. Børvik, O.S. Hopperstad, A. Benallal, Flow and fracture characteristics of aluminium alloy AA5083–H116 as function of strain rate, temperature and triaxiality, Mater. Sci. Eng., A 364 (2004) 260–272.
[23] S. Dey, T. Børvik, O. Hopperstad, J. Leinum, M. Langseth, The effect of target strength on the perforation of steel plates using three different projectile nose shapes, Int. J. Impact Eng. 30 (2004) 1005–1038.
[24] N. Brar, V. Joshi, B. Harris. Constitutive Model Constants for Al7075-t651 and Al7075-t6. SHOCK COMPRESSION OF CONDENSED MATTER 2009: Proceedings of the American Physical Society Topical Group on Shock Compression of Condensed Matter: AIP Publishing; 2009. p. 945-8.
[25] T. Børvik, A.H. Clausen, M. Eriksson, T. Berstad, O.S. Hopperstad, M. Langseth, Experimental and numerical study on the perforation of AA6005-T6 panels, Int. J. Impact Eng. 32 (2005) 35–64.
[26] M. Akbari, S. Buhl, C. Leinenbach, K. Wegener, A new value for Johnson Cook damage limit criterion in machining with large negative rake angle as basis for understanding of grinding, J. Mater. Process. Technol. 234 (2016) 58–71.
[27] Y. Bao, Prediction of ductile crack formation in uncracked bodies, Massachusetts Institute of Technology, 2003.
[28] P.W. Bridgman, Studies in large plastic flow and fracture, McGraw-Hill New York, 1952.
[29] H. Roelofs, N. Renaudot, D. Smolenicki, J. Boos, F. Kuster, The Behaviour of Graphitized Steels in Machining Processes, Mater. Sci. Forum (2017).
[30] Y. Bao, T. Wierzbicki, On fracture locus in the equivalent strain and stress triaxiality space, Int. J. Mech. Sci. 46 (2004) 81–98.
[31] A. Gilioli, A. Manes, M. Giglio, T. Wierzbicki, Predicting ballistic impact failure of aluminium 6061–T6 with the rate-independent Bao-Wierzbicki fracture model, Int. J. Impact Eng. 76 (2015) 207–220.
[32] E. Cadoni, M. Dotta, D. Forni, P. Spätig, Strain-rate behavior in tension of the tempered martensitic reduced activation steel Eurofer97, J. Nucl. Mater. 414 (2011) 360–366.
[33] E. Cadoni, M. Dotta, D. Forni, N. Tesio, C. Albertini, Mechanical behaviour of quenched and self-tempered reinforcing steel in tension under high strain rate, Mater. Des. 49 (2013) 657–666.
[34] E. Cadoni, M. Dotta, D. Forni, Tensile behaviour of reinforcing steels at high strain rate and high temperature, in: Key Engineering Materials, Trans Tech Publ, 2016, pp. 791–798.
[35] D. Forni, B. Chiaia, E. Cadoni, High strain rate response of S355 at high temperatures, Mater. Des. 94 (2016) 467–478.
[36] T. Coleman, Y. Zhang. Optimization toolbox user's guide. Matlab The Mathworks Inc. 2016.
[37] K. Levenberg, A method for the solution of certain non-linear problems in least squares, Q. Appl. Math. 2 (1944) 164–168.
[38] D.W. Marquardt, An algorithm for least-squares estimation of nonlinear parameters, J. Soc. Ind. Appl. Math. 11 (1963) 431–441.
[39] M. Hanke-Bourgeois, Grundlagen der numerischen Mathematik und des wissenschaftlichen Rechnens, Springer, 2009.
[40] W. Sun, Y.-X. Yuan, Optimization theory and methods: nonlinear programming, Springer Science & Business Media, 2006.
[41] Mathworks. Global Optimization Toolbox User's Guide. Matlab The Mathworks Inc. 2016.
[42] D. Kleinbaum. Applied Regression Analysis and Multivariable Methods: Content Technologies, Inc.; 2016.
[43] M. Stevenson, J.D. Campbell, High Strain Rate Testing of a Low Carbon Steel to High Strains over a Range of Temperatures. Using a Torsional Hopkinson-bar Apparatus, Oxford Univ (United Kingdom) Dept of Engineering Science, 1974.
[44] H. Klippel, M. Gerstgrasser, D. Smolenicki, E. Cadoni, H. Roelofs, P. Wegener. Johnson Cook Flow Stress Parameter for Free Cutting Steel 50SiB8. arXiv preprint arXiv:200714087. 2020.
[45] D. Smolenicki, Chip formation analysis of innovative graphitic steel in drilling processes, ETH Zurich (2017).